Progress In Electromagnetics Research C, Vol. 122, 1–15, 2022

FDTD Simulation of a Two-Port Nonlinear Device Characterized by Its *X*-Parameters

Joshua M. Kast* **and Atef Z. Elsherbeni**

Abstract—A new formulation for the finite-difference time-domain (FDTD) technique is presented, for nonlinear circuit components provided that their X-Parameter representations are known. Transient electric fields at specified locations within the FDTD simulation are updated based on the frequency domain behavior of a multi-port nonlinear device, using the X-Parameter behavioral model. The formulation is demonstrated through the simulation of a nonlinear common-emitter amplifier embedded in a microstrip circuit with X-Parameters calculated from SPICE simulation results. Agreement may be seen between the X-Parameter-based simulation results and those acquired using a lumped-element method.

1. INTRODUCTION

We developed a technique for simulating nonlinear devices in the finite-difference time-domain (FDTD) electromagnetic simulation based on their X-Parameters. The FDTD technique simulates microwave circuits by updating the differential form of Maxwell's equations in the time domain, over a 3D domain which has been divided into a grid of rectilinear cells [1]. Based upon previous work in extraction of X-Parameters from FDTD simulations [2, 3] and X-Parameter-based FDTD simulations [4], we develop a modified updating formulation, which is used to represent the behavior of a semiconductor or a nonlinear device, where the nonlinear behavior of the device has been characterized by the X-Parameter representation — a frequency-domain model of nonlinear microwave devices. This work extends that of [4] by allowing multi-port devices to be simulated, and by including the $X^{(S)}$ and $X^{(T)}$ parameters in the updating formulation.

Numerous extensions to FDTD have been developed to address different modeling requirements. For example, the basic FDTD simulations utilize updating formulations for free space, electric conductors, excitation sources, and absorbing boundary conditions. Additional updating formulations have been developed for passive components such as resistors and capacitors, lumped [6] and dependent [7] sources, and active nonlinear components such as BJT [8, 9] and FET [10–12] transistors. Models for nonlinear components vary in their accuracy and computational cost, and all require accurate model parameters to be known for the device being simulated.

The X-Parameters are a recently-developed behavioral model for representing transistors, amplifiers, and other nonlinear microwave devices [13]. In the X-Parameters, nonlinear behavior is described in the frequency-domain by parameters which describe the device's behavior in terms of its large- and small-signal responses linearized around a specified operating point. Whereas the X-Parameters are a frequency-domain formulation, we find that they may be conveniently incorporated into the FDTD simulation's time-stepping formulation.

This novel FDTD formulation for simulation of devices based on their X-Parameters has several possible applications. First, it facilitates the time-domain simulation and optimization of microwave

Received 17 May 2022, Accepted 21 July 2022, Scheduled 2 August 2022
* Corresponding author: Joshua M. Kast (jkast@mines.edu).
The authors are with the Colorado School of Mines, Golden, CO, USA.

circuits composed of components with known X-Parameters, while leveraging the wideband and full-wave characteristics of the FDTD technique. Second, it provides a basis for the evaluation of other FDTD implementations of nonlinear components. The authors are not aware of a similar implementation of the X-Parameters into the FDTD technique.

2. *X*-PARAMETERS

The X-Parameter model estimates the operation of nonlinear components in the context of a microwave circuit [13]. X-Parameter is a behavioral model, meaning that it does not contain information about a device's semiconductor properties or internal geometry, but rather encapsulates measurement data regarding the device's response to input signals [5]. Specifically, the X-Parameter model encapsulates information about voltage waves emitted from the device (denoted as B waves), resulting from waves incident upon the device (A waves). For a nonlinear device under typical application in a microwave system, most of the energy in the A and B waves will be focused around a fundamental operating frequency f_0, with some additional energy present at integer harmonics of f_0: $2f_0$, $3f_0$, etc. Therefore, the X-Parameter model records the B wave response to an A wave stimulus in the frequency domain, at frequencies of kf_0.

Because nonlinear device operation is significantly impacted by factors such as power of the incident waveform and DC bias, X-Parameters are applicable only at a specified operating point, called "Large-Signal Operating Point" ($LSOP$) by the method's authors [13]. The X-Parameter model describes a device's behavior using two sets of terms. The "large-signal" terms, denoted by $X^{(FB)}$, describe the device's operation at the $LSOP$. Meanwhile, the "small-signal" terms, denoted by $X^{(S)}$ and $X^{(T)}$, describe changes to the device's behavior in terms of small perturbations away from the $LSOP$, perhaps due to mismatch at one of the device's ports.

Whereas FDTD simulation operates on electric and magnetic fields, and circuit simulations operate on voltage and current, the microwave X-Parameter model is written in terms of wave quantities. For a given device, the definition of an incoming wave A in terms of its voltage and current is given as [13]:

$$A_{q,l} = \frac{\widetilde{V}_{q,l} + Z_0 \widetilde{I}_{q,l}}{\sqrt{8 \cdot Z_0}}. \tag{1}$$

We note that for this formulation, Z_0 is assumed to be a real number greater than zero, corresponding to a lossless, passive transmission line. This A wave is defined at port q of the device, and at harmonic l, so that the frequency of the wave is $f = lf_0$. The voltage and current are given as phasor values with positive current defined as current flowing into the device. The wave value is normalized by the term $\sqrt{8 \cdot Z_0}$, where Z_0 is the characteristic impedance of the transmission line attached to the device. Note that other normalizations exist, and we choose this one to be consistent with the X-Parameter formulation [13]. Voltage ($\widetilde{V}$) and current ($\widetilde{I}$) are represented as phasor quantities, which are related to the time-domain quantities by the inverse discrete Fourier transform as [14]:

$$V_q(t) = \mathfrak{Re}\left[\sum_{l=1}^{K} \widetilde{V}_{q,l} e^{2\pi j l f_0 t}\right], \tag{2}$$

and similarly for $\widetilde{I}$. For waves flowing outward from the device, an outgoing B is additionally defined [13] for a wave emitted from port p with harmonic k:

$$B_{p,k} = \frac{\widetilde{V}_{p,k} - Z_0 \widetilde{I}_{p,k}}{\sqrt{8 \cdot Z_0}}. \tag{3}$$

In terms of these wave quantities, the X-Parameter model [13] relates B waves to A waves for a device with N ports and at K harmonics, at a fundamental frequency f_0 and operating conditions $LSOP$ as follows:

$$B_{p,k} \cong X^{(FB)}_{p,k}(LSOP) P^k + \sum_{\substack{q=1 \\ l=1 \\ (q,l)\neq(1,1)}}^{\substack{q=N \\ l=K}} \begin{pmatrix} X^{(S)}_{p,k;q,l}(LSOP) A_{q,l} P^{k-l} \\ + X^{(T)}_{p,k;q,l}(LSOP) A^*_{q,l} P^{k+l} \end{pmatrix}. \tag{4}$$

In this equation, we note that the parameter $X^{(FB)}_{p,k}$ is defined at each port p and harmonic k. Further, the parameters $X^{(S)}_{p,k;q,l}$ and $X^{(T)}_{p,k;q,l}$ are defined for each combination of input and output ports and harmonics. Note that $X^{(S)}_{p,k;1,1}$ and $X^{(T)}_{p,k;1,1}$ are not defined. As the A wave at port 1, harmonic 1 is the "large-signal" incoming wave, and small perturbations upon this are not considered in this model. The variable P is a phase-normalization constant with value:

$$P = e^{j\angle A_{1,1}}. \tag{5}$$

This value P is required to ensure that phases remain commensurate across frequencies.

Values of $X^{(FB)}_{p,k}$ are determined by placing the device into a condition where all $A_{q,l}$ except $A_{1,1}$ are set to zero (the $LSOP$ condition) and finding the values of $B_{p,k}$ at each port and harmonic. Values of $X^{(S)}_{p,k;q,l}$ and $X^{(T)}_{p,k;q,l}$ are determined by placing the device in the $LSOP$ condition, then applying small additional $A_{q,l}$ stimuli and calculating:

$$X^{(S)}_{p,k;q,l} \simeq \left.\frac{\partial B_{p,k}}{\partial \left(A_{q,l}P^{-l}\right)}\right|_{LSOP}, \tag{6}$$

and

$$X^{(T)}_{p,k;q,l} \simeq \left.\frac{\partial B_{p,k}}{\partial \left(A_{q,l}P^{-l}\right)^*}\right|_{LSOP}. \tag{7}$$

In the laboratory, the X-Parameters are ideally measured using instrumentation such as a large-signal network analyzer (LSNA), which can simultaneously provide the stimulus waveforms and measure the device's response. We have previously demonstrated that X-Parameter may be determined from FDTD simulation data where voltage and current quantities are known [2, 3]. Methods for extracting X-Parameters from laboratory measurement data are well described in [13]. There is any uncertainty in the extracted data, and the development of a fuzzy extraction procedure could be considered.

3. FDTD UPDATING FORMULATION

In the FDTD technique, the simulation domain is segmented into a grid, with the electric and magnetic fields being calculated at each cell within this grid. The electric field ($\vec{E}$) is related to the magnetic field ($\vec{H}$) and current density ($\vec{J}$) by [15]:

$$\nabla \times \vec{H} = \varepsilon \frac{\partial \vec{E}}{\partial t} + \vec{J}, \tag{8}$$

where ε is the electric permittivity. Conversely, magnetic field is related to electric field and magnetic current density ($\vec{M}$) by:

$$\nabla \times \vec{E} = -\mu \frac{\partial \vec{H}}{\partial t} - \vec{M}, \tag{9}$$

with μ as the electric permittivity.

We formulate (8) for use in the FDTD simulation by replacing the partial derivative and curl operators by the second-order finite differences. Fields are evaluated at each location i, j, k along a 3D grid, for N_{step} time steps. The FDTD grid is defined by cell-spacings Δx, Δy, and Δz, in x, y, and z Cartesian coordinates, respectively, and the simulation time-step increment is specified by Δt. For example, (8) can be represented as an updating equation, by using the notation of [1]:

$$\begin{aligned} \varepsilon_z|_{i,j,k} \frac{E_z|^{n+1}_{i,j,k} - E_z|^{n}_{i,j,k}}{\Delta t} = & - J_z|^{n+\frac{1}{2}}_{i,j,k} \\ & + \frac{H_y|^{n+\frac{1}{2}}_{i,j,k} - H_y|^{n+\frac{1}{2}}_{i-1,j,k}}{\Delta x} \\ & - \frac{H_x|^{n+\frac{1}{2}}_{i,j,k} - H_x|^{n+\frac{1}{2}}_{i,j-1,k}}{\Delta y}. \end{aligned} \tag{10}$$

This equation allows the electric field at time step $n+1$, using magnetic fields and current calculated at $n+\frac{1}{2}$, and it is applicable to regions with zero electric conductivity. A modified version of (10) is used for electrically-conducting regions, and it is well described in the literature. For the specific location of our X-Parameter updating formulation, we will assume that the electric conductivity $\sigma^e = 0$.

To reduce the size of the notation, we define the symbol $\boxed{\nabla \times H}_z$ to indicate part of the updating equation computed from the curl of the surrounding H fields normal to the z direction:

$$\begin{aligned}\boxed{\nabla \times H}_z\Big|_{i,j,k}^{n+\frac{1}{2}} = \; & \frac{H_y\big|_{i,j,k}^{n+\frac{1}{2}} - H_y\big|_{i-1,j,k}^{n+\frac{1}{2}}}{\Delta x} \\ & - \frac{H_x\big|_{i,j,k}^{n+\frac{1}{2}} - H_x\big|_{i,j-1,k}^{n+\frac{1}{2}}}{\Delta y}.\end{aligned} \tag{11}$$

Applying (11) to (10) yields:

$$\varepsilon_z\big|_{i,j,k} \frac{E_z\big|_{i,j,k}^{n+1} - E_z\big|_{i,j,k}^{n}}{\Delta t} = -\, J_z\Big|_{i,j,k}^{n+\frac{1}{2}} + \boxed{\nabla \times H}_z\Big|_{i,j,k}^{n+\frac{1}{2}}. \tag{12}$$

3.1. Wave Representation within FDTD

We have already defined the wave quantities A and B in (1) and (3), respectively. We now must adapt these to the time domain. At a given port p and time step $n+\frac{1}{2}$, we may find the A wave quantity as:

$$\breve{A}_p\big|^{n+\frac{1}{2}} = \frac{V_p\big|^{n+\frac{1}{2}} + Z_0 I_p\big|^{n+\frac{1}{2}}}{\sqrt{8 \cdot Z_0}}. \tag{13}$$

We use the accent mark $\breve{}$ to indicate time-domain for quantities which are normally expected to be frequency domain such as the A and B waves. To calculate this time-domain $\breve{A}$ quantity, we must know the voltage V_p and current I_p at port p. Voltage may be calculated from the electric field as:

$$V_p\big|^{n+\frac{1}{2}} = -\frac{E_z\big|_{i,j,k}^{n+\frac{1}{2}}}{\Delta z}. \tag{14}$$

Because $E_z\big|_{i,j,k}^{n+\frac{1}{2}}$ is not known directly in the simulation, the voltage is calculated using the average of the electric fields at steps n and $n+1$:

$$V_p\big|^{n+\frac{1}{2}} = -\frac{E_z\big|_{i,j,k}^{n} + E_z\big|_{i,j,k}^{n+1}}{\Delta z}. \tag{15}$$

We may now find the z-directed current at location i, j, k. Current is related to current density by $I_z\big|^{n+\frac{1}{2}} = J_z\big|_{i,j,k}^{n+\frac{1}{2}} \Delta x \Delta y$. This relationship may be inserted into (12), and then solved for current, giving:

$$I_z\Big|_{i,j,k}^{n+\frac{1}{2}} = -\,\varepsilon_z\big|_{i,j,k} \Delta x \Delta y \frac{E_z\big|_{i,j,k}^{n+1} - E_z\big|_{i,j,k}^{n}}{\Delta t} + \Delta x \Delta y \boxed{\nabla \times H}_z\Big|_{i,j,k}^{n+\frac{1}{2}}. \tag{16}$$

We insert (15) and (16) into (13), giving an equation for the time-domain $\breve{A}$ wave:

$$\begin{aligned}\breve{A}_p\big|^{n+\frac{1}{2}} = & -\frac{E_z\big|_{i,j,k}^{n} + E_z\big|_{i,j,k}^{n+1}}{\Delta z \sqrt{8 \cdot Z_0}} \\ & - Z_0 \frac{-\varepsilon_z\big|_{i,j,k} \Delta x \Delta y \frac{E_z\big|_{i,j,k}^{n+1} - E_z\big|_{i,j,k}^{n}}{\Delta t} + \Delta x \Delta y \boxed{\nabla \times H}_z\Big|_{i,j,k}^{n+\frac{1}{2}}}{\sqrt{8 \cdot Z_0}} \\ = & \, C_p^{A1} E_z\big|_{i,j,k}^{n+1} + C_p^{A2} E_z\big|_{i,j,k}^{n} + C_p^{A3} \boxed{\nabla \times H}_z\Big|_{i,j,k}^{n+\frac{1}{2}}\end{aligned} \tag{17}$$

Note the change of sign for the current term. This is because the density J_z is directed in the $+z$ direction. However, we will define current going *into* the device to be in the $-z$ direction. The constants C_p^{A1}, C_p^{A2}, and C_p^{A3} are used to maintain a compact representation and are defined as:

$$C_p^{A1} = -\frac{1}{\Delta z\sqrt{8\cdot Z_0}} + \frac{\varepsilon_z|_{i,j,k}\Delta x\Delta y}{\Delta t\Delta z\sqrt{8\cdot Z_0}}$$
$$C_p^{A2} = -\frac{1}{\Delta z\sqrt{8\cdot Z_0}} - \frac{\varepsilon_z|_{i,j,k}\Delta x\Delta y}{\Delta t\Delta z\sqrt{8\cdot Z_0}}$$
$$C_p^{A3} = -\frac{\Delta x\Delta y}{\Delta z\sqrt{8\cdot Z_0}}.$$

A similar formulation may be made for the outgoing $\breve{B}$ wave as:

$$\breve{B}_p|^{n+\frac{1}{2}} = C_p^{B1}E_z|_{i,j,k}^{n+1} + C_p^{B2}E_z|_{i,j,k}^{n} + C_p^{B3}\boxed{\nabla\times H}_z|_{i,j,k}^{n+\frac{1}{2}}, \tag{18}$$

with:

$$C_p^{B1} = -\frac{1}{\Delta z\sqrt{8\cdot Z_0}} - \frac{\varepsilon_z|_{i,j,k}\Delta x\Delta y}{\Delta t\Delta z\sqrt{8\cdot Z_0}}$$
$$C_p^{B2} = -\frac{1}{\Delta z\sqrt{8\cdot Z_0}} + \frac{\varepsilon_z|_{i,j,k}\Delta x\Delta y}{\Delta t\Delta z\sqrt{8\cdot Z_0}}$$
$$C_p^{B3} = \frac{\Delta x\Delta y}{\Delta z\sqrt{8\cdot Z_0}}.$$

3.2. *X*-Parameter Based Updating Formulation

The previous equations are the foundation for an X-Parameter-based updating formulation for an FDTD cell. The goal of this formulation is to update the electric field $E_z|_{i,j,k}^{n+1}$ at port p by using the relationship of A and B waves of (4). To maintain compatibility within the FDTD formulation in [1], this formulation must occupy a single Yee-grid cell for each device port and maintain a 2nd-order accuracy by means of central-difference approximations. We start by writing a formulation for time-domain $\breve{B}$ waves in terms of frequency-domain B waves as:

$$\breve{B}_p|^{n+\frac{1}{2}} = \mathfrak{Re}\left[\sum_{k=1}^{K} B_{p,k}e^{2\pi jkf_0\Delta t\left(n+\frac{1}{2}\right)}\right]. \tag{19}$$

We will additionally need an inverse transform — a means to convert time-domain field quantities into a frequency-domain A wave as:

$$A_{q,l} = \sum_{n_{\text{step}}=n-N_W}^{n}\left(C_q^{A1}E_z|_q^{n_{\text{step}}+1} + C_q^{A2}E_z|_q^{n_{\text{step}}} + C_q^{A3}\boxed{\nabla\times H}_z|_q^{n_{\text{step}}+\frac{1}{2}}\right)\frac{e^{2\pi jlf_0\Delta tn_{\text{step}}}}{N_W}. \tag{20}$$

Here, n is the current time step, and N_W is the number of preceding time steps over which the A waves are calculated. Typically N_W should be selected so that $N_W = (f_0\Delta t)^{-1}$, such that one period of the fundamental waveform will be captured in each calculation. We then insert (4) into (19), removing the $(LSOP)$ notation for compactness (the operating point will be specified in the text where applicable):

$$\breve{B}_p|^{n+\frac{1}{2}} = \mathfrak{Re}\left[\sum_{k=1}^{K}\left(X_{p,k}^{(FB)}P^k + \sum_{\substack{q=1\\(q,l)\neq(1,1)}}^{\substack{q=N\\l=K}}\begin{pmatrix}X_{p,k;q,l}^{(S)}A_{q,l}P^{k-l}\\ +X_{p,k;q,l}^{(T)}A_{q,l}^{*}P^{k+l}\end{pmatrix}\right)e^{2\pi jkf_0\Delta t\left(n+\frac{1}{2}\right)}\right]. \tag{21}$$

We then replace the wave $\breve{B}_p$ by its time-domain definition in (18) and the wave $A_{q,l}$ by the representation in (20):

$$\breve{B}_p|^{n+\frac{1}{2}} = \mathfrak{Re}\left[\sum_{k=1}^{K} X_{p,k}^{(FB)} P^k e^{2\pi j k f_0 \Delta t\left(n+\frac{1}{2}\right)} + \sum_{\substack{k=1\\q=1\\l=1\\(q,l)\neq(1,1)}}^{\substack{k=K\\q=N\\l=K}} \begin{pmatrix} X_{p,k;q,l}^{(S)} A_{q,l} P^{k-l} e^{2\pi j k f_0 \Delta t\left(n+\frac{1}{2}\right)} \\ +X_{p,k;q,l}^{(T)} A_{q,l}^{*} P^{k+l} e^{2\pi j k f_0 \Delta t\left(n+\frac{1}{2}\right)} \end{pmatrix}\right]. \tag{22}$$

Inserting (18) into (22) gives:

$$\begin{pmatrix} C_p^{B1} E_z|_{i,j,k}^{n+1} \\ +C_p^{B2} E_z|_{i,j,k}^{n} \\ +C_p^{B3} \boxed{\nabla \times H}_z|_{i,j,k}^{n+\frac{1}{2}} \end{pmatrix} = \mathfrak{Re}\left[\sum_{k=1}^{K} X_{p,k}^{(FB)} P^k e^{2\pi j k f_0 \Delta t\left(n+\frac{1}{2}\right)}\right.$$
$$\left. + \sum_{\substack{k=1\\q=1\\l=1\\n_{\text{step}}=n-N_W\\(q,l)\neq(1,1)}}^{\substack{k=K\\q=N\\l=K\\n_{\text{step}}=n}} \frac{\begin{pmatrix} X_{p,k;q,l}^{(S)} P^{k-l} e^{2\pi j f_0 \Delta t\left(k n+\frac{k}{2}+l n_{\text{step}}\right)} \\ +X_{p,k;q,l}^{(T)} P^{k+l} e^{2\pi j f_0 \Delta t\left(k n+\frac{k}{2}-l n_{\text{step}}\right)} \end{pmatrix}}{N_W} \begin{pmatrix} C_q^{A1} E_z|_q^{n_{\text{step}}+1} \\ +C_q^{A2} E_z|_q^{n_{\text{step}}} \\ +C_q^{A3} \boxed{\nabla \times H}_z|_q^{n_{\text{step}}+\frac{1}{2}} \end{pmatrix}\right]. \tag{23}$$

From (23), we see that the electric field $E_z|_{i,j,k}^{n+1}$ is the unknown variable in a linear system of equations, which can be formulated as:

$$\mathbf{M}\vec{x} = \vec{b}, \tag{24}$$

where $\mathbf{M}$ is a matrix of size $N \times N$, and $\vec{x}$ and $\vec{b}$ are vectors of length N, corresponding to a device with N ports. The unknown electric fields are elements of the vector $\vec{x}$:

$$x_p = E_z|_p^{n_{\text{step}}+1}. \tag{25}$$

We find the values of $\mathbf{M}$ as:

$$M_{p,q} = \begin{cases} C_p^{B1} - \mathfrak{Re}\left[\sum_{\substack{k=1\\l=1}}^{\substack{k=K\\l=K}} \begin{pmatrix} X_{p,k;q,l}^{(S)} P^{k-l} C_q^{A1} e^{2\pi j f_0\left(k n_{\text{step}}+\frac{k}{2}+l n_{\text{step}}\right)} \\ +X_{p,k;q,l}^{(T)} P^{k+l} C_q^{A1} e^{2\pi j f_0\left(k n_{\text{step}}+\frac{k}{2}-l n_{\text{step}}\right)} \end{pmatrix}\right], & \text{if } p=q \\ -\mathfrak{Re}\left[\sum_{\substack{k=1\\l=1}}^{\substack{k=K\\l=K}} \begin{pmatrix} X_{p,k;q,l}^{(S)} P^{k-l} C_q^{A1} e^{2\pi j f_0\left(k n_{\text{step}}+\frac{k}{2}+l n_{\text{step}}\right)} \\ +X_{p,k;q,l}^{(T)} P^{k+l} C_q^{A1} e^{2\pi j f_0\left(k n_{\text{step}}+\frac{k}{2}-l n_{\text{step}}\right)} \end{pmatrix}\right], & \text{otherwise.} \end{cases} \tag{26}$$

Values in the vector $\vec{b}$ are then found as:

$$
\begin{aligned}
b_p = \; \mathfrak{Re}\Bigg\{ & \sum_{k=1}^{K} X_{p,k}^{(FB)} P^k e^{2\pi j k f_0 \Delta t\left(n_{\text{step}}+\frac{1}{2}\right)} \\
& + \sum_{\substack{k=K \\ q=N \\ l=K \\ n_{\text{step}}=n-1 \\ k=1 \\ q=1 \\ l=1 \\ n_{\text{step}}=n-N_W \\ (q,l)\neq(1,1)}} \frac{\begin{pmatrix} X_{p,k;q,l}^{(S)} P^{k-l} e^{2\pi j f_0 \Delta t\left(kn+\frac{k}{2}+ln_{\text{step}}\right)} \\ +X_{p,k;q,l}^{(T)} P^{k+l} e^{2\pi j f_0 \Delta t\left(kn+\frac{k}{2}-ln_{\text{step}}\right)} \end{pmatrix}}{N_W} \begin{pmatrix} C_q^{A1} E_z|_q^{n_{\text{step}}+1} \\ +C_q^{A2} E_z|_q^{n_{\text{step}}} \\ +C_q^{A3} \boxed{\nabla \times H}_z|_q^{n_{\text{step}}+\frac{1}{2}} \end{pmatrix} \\
& + \sum_{\substack{k=K \\ q=N \\ l=K \\ k=1 \\ q=1 \\ l=1 \\ (q,l)\neq(1,1)}} \frac{\begin{pmatrix} X_{p,k;q,l}^{(S)} P^{k-l} e^{2\pi j f_0 \Delta t\left(kn+\frac{k}{2}+ln\right)} \\ +X_{p,k;q,l}^{(T)} P^{k+l} e^{2\pi j f_0 \Delta t\left(kn+\frac{k}{2}-ln\right)} \end{pmatrix}}{N_W} \begin{pmatrix} C_q^{A2} E_z|_q^{n} \\ + C_q^{A3} \boxed{\nabla \times H}_z|_q^{n+\frac{1}{2}} \end{pmatrix} \Bigg\} \\
& - C_p^{B2} E_z|_{i,j,k}^{n} - C_p^{B3} \boxed{\nabla \times H}_z|_{i,j,k}^{n+\frac{1}{2}}.
\end{aligned}
\tag{27}
$$

We therefore find that the X-Parameter representation of a nonlinear component may be embedded within an FDTD updating equation, and that this updating equation requires only the solution of an $N \times N$ matrix for each simulation time step — no iterative solutions to nonlinear equations are required. Some interesting properties of the matrix $\mathbf{M}$: First, the values of C_p^{B1} along the diagonal of $\mathbf{M}$ are the dominant components of this matrix, and in the case of $X^{(S)}$ and $X^{(T)}$ (no small-signal interactions), the matrix $\mathbf{M}$ becomes purely diagonal. Second, the condition number of $\mathbf{M}$ increases as $X^{(S)}$ or $X^{(T)}$ increase, and decreases as N_W increases. Thus, accuracy of the solution can be improved by decreasing the time step Δt. For two-port devices, $\mathbf{M}$ will have size 2×2, allowing for a closed-form solution with no matrix inversion.

4. FDTD SIMULATIONS

The formulation described in the previous section was tested in the context of an FDTD simulation of a common-emitter amplifier based on a bipolar-junction transistor (BJT). First, the amplifier design, illustrated in Fig. 1 was implemented in FDTD simulation, with the simulation domain shown in Fig. 2. Next, the circuit in Fig. 1 was simulated in the ngSPICE circuit simulator [16], with ideal $50\,\Omega$ source and load at the RF ports. The SPICE simulation is necessary to establish the X-Parameters of the transistor circuit. Finally, the X-Parameters calculated from the SPICE simulation results are used to perform the time-domain simulation of the amplifier circuit. We demonstrate the effectiveness of the X-Parameter-based FDTD updating formulation by comparison to the BJT amplifier simulated using lumped-element FDTD techniques [1, 8].

4.1. FDTD Lumped-Element Simulation

To provide a basis for comparison, a BJT common-emitter amplifier was implemented for FDTD simulation as shown in Fig. 2. Microstrip transmission lines on either side of the amplifier are designed for $50\,\Omega$ impedance and are attached to $50\,\Omega$ ports at the edges of the microstrip substrate. The BJT

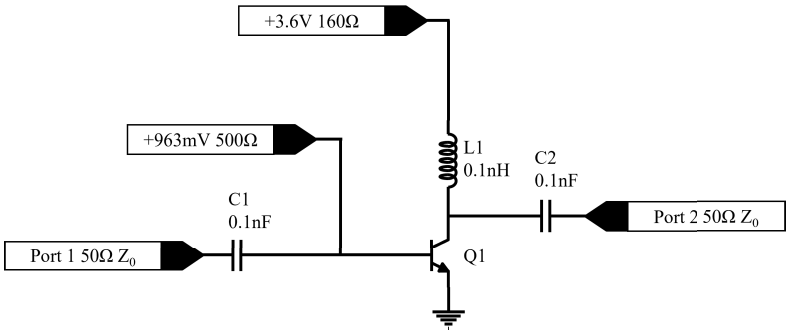

Figure 1. Schematic diagram of the simulated common-emitter BJT amplifier. Capacitors are present to block DC current, while the inductor at the transistor's collector terminal reduces RF current into the power supply.

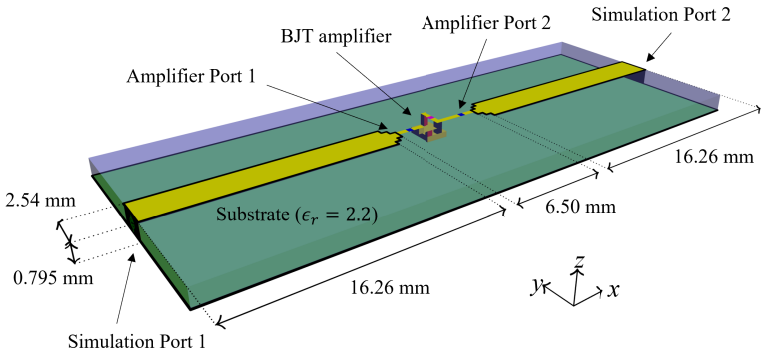

Figure 2. Diagram of FDTD simulation domain for common-emitter BJT amplifier. Segments of conductive (microstrip) transmission line are shown in yellow, and are surmounted on a dielectric substrate shown in translucent blue. Components of the amplifier are embedded within this substrate as shown at the center of the image. A conductive ground plane is shown in green and provides a current return path for the microstrip transmission line.

amplifier, shown in Fig. 1, is implemented using simulated lumped-element components and is illustrated in detail in Fig. 3. Updating formulations for the resistor and inductor are described in [1], and the updating formulation for the BJT transistor is based on the Ebers-Moll model and described in [8]. Because the model for the BJT transistor is only valid across single cells, tapered segments are placed between the transmission-line segments and the amplifier circuit.

The FDTD simulation is performed with cell sizes of $\Delta x = 406.4\,\mu\text{m}$, $\Delta y = 423.3\,\mu\text{m}$, and $\Delta z = 265\,\mu\text{m}$. The simulation time step is set to 0.5 ps. On five sides (all directions except $-z$), the simulation is bounded by 10 cells of air buffer layer followed by 8 cells of CPML absorbing boundary. In the $-z$ direction, the simulation is bounded by a conducting layer at the same location as the microstrip's ground plane. It takes at least 175 ns for the transistor's bias voltage to stabilize, meaning that a minimum of 350,000 simulation time steps are required in order to properly observe the amplifier's behavior. The amplifier was evaluated with a 100 MHz excitation waveform at several different voltages.

4.2. SPICE Circuit Simulation

The amplifier circuit of Fig. 1 was simulated in the ngSPICE simulation package to determine its large-signal $X^{(FB)}$ characteristics and its small-signal $X^{(S)}$ and $X^{(T)}$ behavior. A transient simulation was chosen, with a sufficient length to capture the amplifier's behavior after it reached a steady DC state. For the large-signal analysis, the $LSOP$ excitation was a 100 MHz sine wave applied at port 1 of the simulation, at 0.1 mV, 1 mV, 10 mV, and 100 mV, with both simulation ports matched to 50 Ω

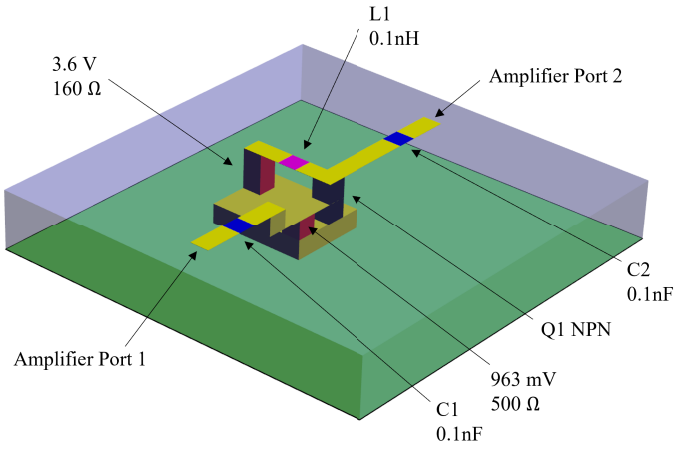

Figure 3. Enlarged view of BJT common-emitter amplifier, detailing FDTD-simulated lumped-elements corresponding to the schematic shown in Fig. 1. Voltage sources are shown in dark red, capacitors in blue, and inductors are magenta.

impedance. For the small-signal analysis, additional simulations were performed: small additional excitations were applied in the form of harmonic frequencies applied at either simulation port, with a magnitude of 1% of the fundamental-frequency excitation voltage. From these simulation results, X-Parameter data were extracted following the approach outlined in [2, 3, 13]. X-Parameter data were extracted to $K = 5$ harmonics. We note that data acquired for a given $LSOP$ are valid only for devices or simulations operating under that same $LSOP$, so X-Parameters determined for a 1mV excitation voltage cannot be used to determine the device behavior at 10 mV or 100 mV.

4.3. FDTD Simulation with *X*-Parameter Updating Formulation

To test the formulation described in Section 3, a new simulation domain was created, where the BJT common-emitter amplifier was replaced by a two-port X-Parameter-based updating formulation, as illustrated in Fig. 4. All other details of the simulation, such as the transmission lines and substrate, were kept identical to those shown in Fig. 2. The updating formulation was provided with X-Parameters as described in Section 4.2. The phase-normalization coefficient P was determined for the X-Parameter updating by applying a 100 MHz excitation waveform, recording voltage and current across port 1 of the amplifier, and calculating the phase of the incoming A wave.

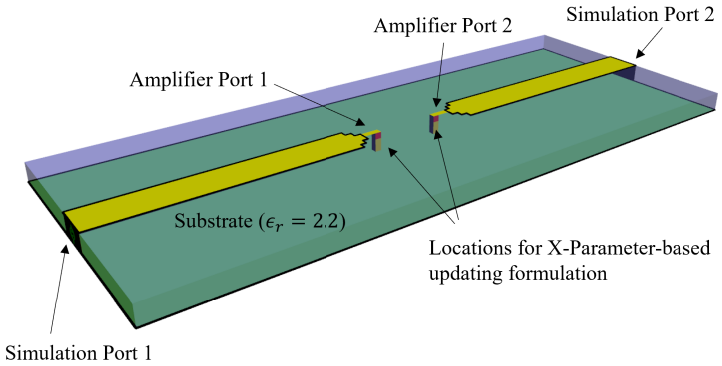

Figure 4. Microstrip simulation domain similar to that of Fig. 2 with BJT amplifier replaced by cells updated based on X-Parameter formulation.

5. RESULTS

5.1. FDTD Lumped-Element Simulation

We simulated the BJT common-emitter amplifier, as shown in Fig. 2, to test the functionality of the amplifier and to provide a basis for comparison for later simulations using the X-Parameter updating formulation. Results from this simulation are plotted in Fig. 5. During the simulation, the 100 MHz excitation waveform is supplied at Simulation Port 1 starting at 0 ns. Additionally, the 3.6 V and 963 mV DC bias voltage sources are enabled at the beginning of the simulation. Due to the presence of inductors and capacitors in the transistor's DC-bias circuit, it takes time for the base and collector voltages to stabilize. In the plot of 5, we see that it takes around 100 ns for a sinusoidal output to begin from the amplifier, and that this output does not stabilize until nearly 200 ns. This behavior is expected for the bias network used — the specific time required for stabilization may be controlled by selecting values of the capacitors and inductors used.

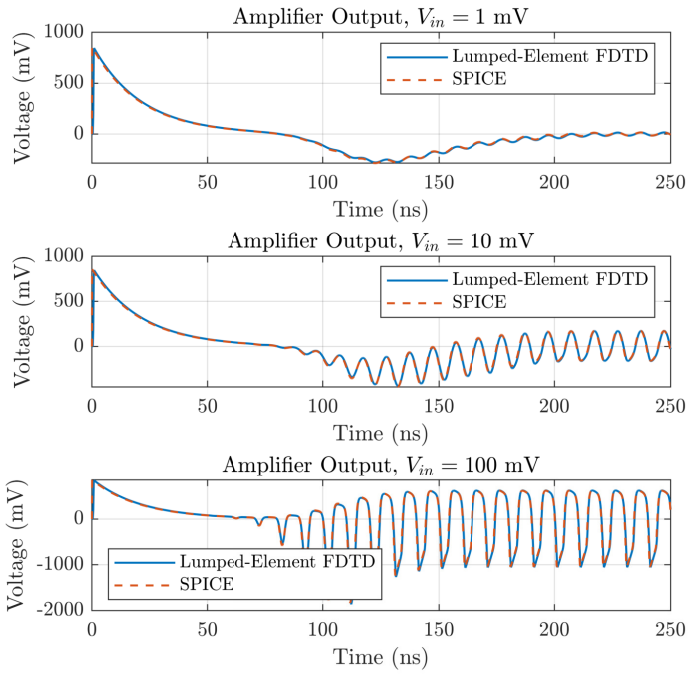

Figure 5. Output (Simulation Port 2) voltage of BJT amplifier for three input (Simulation Port 1) excitation voltages: 1 mV, 10 mV, and 100 mV.

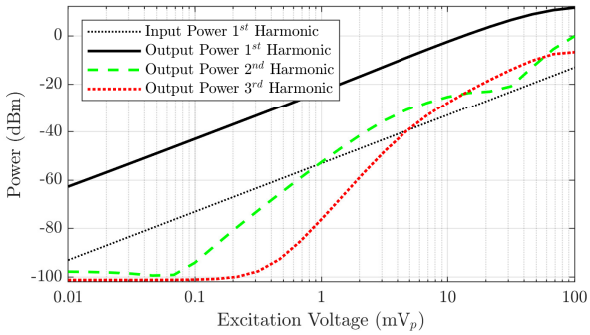

Figure 6. Output (Simulation Port 2) power and harmonics for a range of input (Simulation Port 1) excitation voltages between 0.1 and 100 mV$_p$.

Examining the first plot in 5, we see that after 200 ns, the amplifier produces a stable sinusoidal output of approximately $16\,\mathrm{mV}_p$. As excitation voltage is increased to $10\,\mathrm{mV}_p$, the voltage at the amplifier's output increases to approximately $170\,\mathrm{mV}_p$, and a slight distortion of the waveform can be observed. Finally, when the excitation voltage is increased to $100\,\mathrm{mV}_p$, significant clipping and distortion of the amplified waveform is present. The nonlinear behavior of the amplifier is summarized in the plot of Fig. 6, which was generated from a series of FDTD simulations with the amplifier under a range of input voltages. For input voltages below approximately 0.1 mV, there is minimal presence of the 2nd and 3rd harmonics. As excitation voltage is increased, the powers of the 2nd and 3rd harmonics increase. Peak gain of the amplifier is 30.8 dB, achieved at $6.8\,\mathrm{mV}_p$ excitation — above this voltage, the gain decreases, and harmonics become significant.

5.2. SPICE Circuit Simulation

In addition to the lumped-element FDTD simulation of the amplifier, a circuit-model SPICE simulation was performed. Results from this SPICE simulation were used to calculate X-Parameters for the BJT amplifier as described in Section 4.2. Therefore, we aim for good agreement between the SPICE and lumped-element FDTD simulations. SPICE simulation results are overlaid with corresponding FDTD results in Fig. 5. We see good agreement between the FDTD and SPICE results; however, a constant time offset is observed, with the FDTD result being delayed by approximately 287 ps relative to the SPICE result. There are two sources of this offset: first, SPICE models connections between circuit components as infinitely-short conductors, whereas in FDTD, these conductors have finite length. Second, 50 Ω sources and loads in SPICE are modeled as series resistors with no parasitic or fringing effects, whereas FDTD sources and loads are subject to these nonidealities.

5.3. FDTD Simulation with *X*-Parameter Updating Formulation

We finally tested the FDTD simulation using the proposed X-Parameter-based updating formulation. X-Parameters were computed from SPICE simulation results as described in Section 2. These X-Parameters were then supplied to the updating algorithm, and the simulation program run. An example output voltage of the X-Parameter-based FDTD simulation is plotted in Fig. 7, for an excitation voltage of 10 mV. In comparison to the BJT simulation result, the X-Parameter-based simulation stabilizes very quickly — within two waveform cycles. In the X-Parameter-based simulation, DC bias voltage is not directly considered, so no simulation time is taken for the stabilization of the DC circuit. Rather, the initial inaccuracies are because the algorithm calculates B-waves based on previous timepoints.

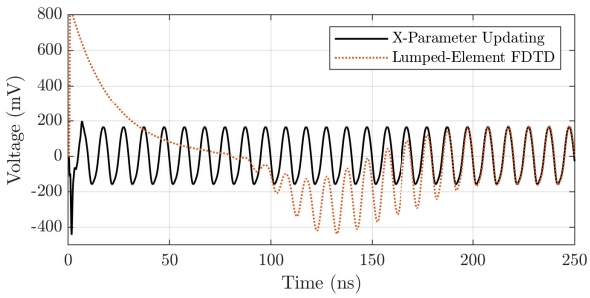

Figure 7. Output voltages from lumped-element FDTD simulation and X-Parameter-based FDTD simulation of BJT amplifier, with excitation voltage of 10 mV.

In general, the X-Parameters describe the operation of a nonlinear device at conditions near the *LSOP* — the operating point at which the X-Parameters were measured or specified. Therefore, the transient response at the device's startup is not considered by our X-Parameter-based FDTD simulation. For some simulations, this attribute may be desirable, as the RF steady state is quickly achieved without a long simulation time. However, for simulations where longer-term dynamic nonlinearities are of interest, an extension to the X-Parameters may need to be introduced.

From Fig. 8, we can see good agreement in the steady-state result of the X-Parameter and lumped-element FDTD simulations. However, a time shift is observed between the lumped-element and X-Parameter results of approximately 287 ps. This is the same difference as observed between the FDTD and SPICE results of Fig. 5. To prove that this difference is a result of the X-Parameters used in the simulation and not the X-Parameter-based FDTD updating algorithm, we repeated the simulation shown in Fig. 8, except with X-Parameters derived from an FDTD simulation of only the lumped-element amplifier at the center 6.5 mm of the domain shown in Fig. 2. In this simulation, the time delay between the two waveforms is reduced to a negligible amount. The accurate result of the simulation is strongly dependent on the accuracy of the supplied X-Parameters.

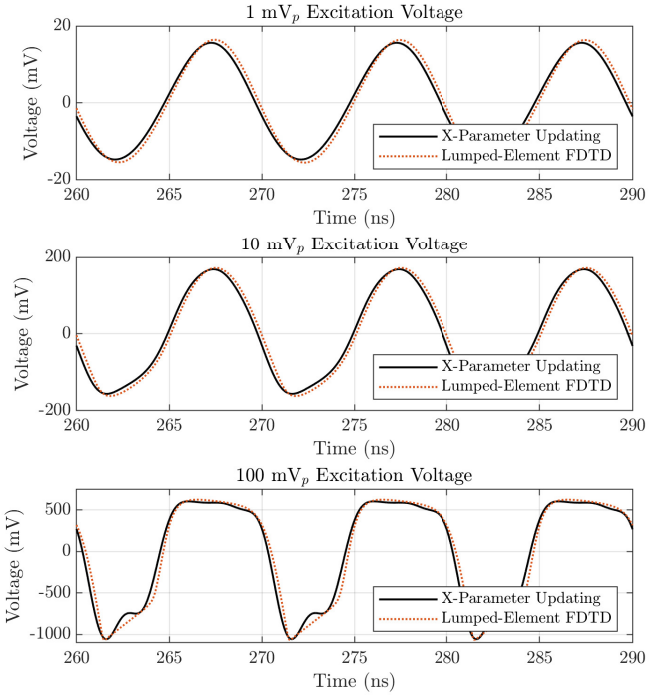

Figure 8. Output (simulation port 2) voltages from lumped-element FDTD simulation and X-Parameter-based FDTD simulation of BJT amplifier, time-aligned to facilitate comparison of results.

In Fig. 8, the experiment was repeated for three different excitation waveform voltages: 1 mV$_p$, 10 mV$_p$, and 100 mV$_p$. For excitation voltages of 1 mV$_p$ and 10 mV$_p$, the X-Parameter based result aligns well with that of the lumped-element FDTD result. At 10 mV, distortion begins to appear in the output waveform, and this effect is captured by the X-Parameter formulation. As excitation voltage is further increased, nonlinear effects are further increased, and some deviation can be observed between the simulation results. In Fig. 8, we notice a discrepancy between the simulation results for the 100 mV excitation voltage. We confirm that this is a result of the SPICE simulation used to produce the X-Parameters and not due to the X-Parameter-based FDTD updating formulation.

The X-Parameters are a frequency-domain model, which capture the behavior of a nonlinear device in terms of the harmonics it generates in response to input waveforms. In Fig. 9, we plot the spectrum of the outgoing B_2 wave at the output (Simulation Port 2) of the amplifier. Good agreement is seen between the amplitudes of the harmonics produced using the two different simulation approaches at frequencies up to 500 MHz, which is the highest harmonic included in the X-Parameters that we calculated. The phase results were also compared between the two techniques. Note that phase is not defined for 0 MHz and is therefore not plotted. A constant time offset of 287 ns was applied to the phase results for the X-Parameter updating based simulation, as this offset was determined to be a result of the SPICE simulation and not the X-Parameter-based updating formulation. Good agreement between frequency-

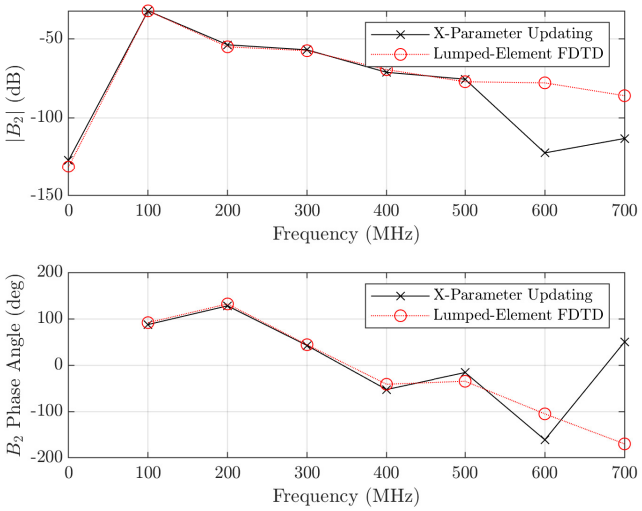

Figure 9. Frequency-domain representation of the output waveform (B_2) of the BJT amplifier under $10\,\mathrm{mV}_p$ excitation, as measured at Simulation Port 2.

domain results of the X-Parameter-based updating formulation and the lumped-element-based FDTD simulation supports the use of the X-Parameter-based approach.

We additionally compared X-Parameter results, which were calculated from the time-domain FDTD simulation results as described in Section 4.2. Examples of the X-Parameter results from the X-Parameter-based FDTD and lumped-element-based FDTD simulations are plotted in Fig. 10. The upper plot is of the parameter $X^{(S)}_{2,k,1,3}$: the change in the signal at the output port (Simulation Port 2), harmonic k, due to a small change in the signal at the input port (Simulation Port 1) at the 3rd harmonic. As expected, the largest change is at harmonic $k = 3$: applying a small 300 MHz signal to the amplifier's input, in addition to the 100 MHz large-signal excitation, produces an amplified 300 MHz signal at the amplifier's output. The bottom plot of Fig. 10 shows the parameter $X^{(S)}_{2,k,1,5}$ with a similar result: application of a small 5th-harmonic component to the excitation signal leads to an increase in 5th-harmonic amplitude (as well as other harmonics) at the output.

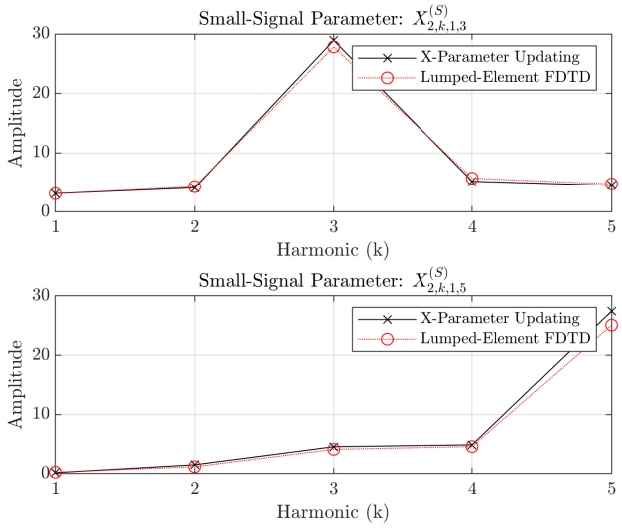

Figure 10. Small-Signal parameter results ($X^{(S)}_{2,k,1,3}$ and $X^{(S)}_{2,k,1,5}$) for BJT amplifier under $10\,\mathrm{mV}_p$ excitation.

The FDTD simulations were performed on an Intel Xeon processor operating at 2.6 GHz. The X-Parameter-based FDTD simulation required 182 ms per FDTD time step, corresponding to a simulation rate of 0.80 MCPS (million cells per second). In contrast, the lumped-element simulation, with the same number of cells and domain size, required 40 ms per FDTD time step: a rate of 3.59 MCPS. At present, the optimization of the X-Parameter-based code has not been fully explored. Specific possible targets for optimization include performing the discrete Fourier transform on a limited subset of the previous sampled A-wave values and optimizing the data structure into which electric- and magnetic-field data are stored. Additionally, the Fourier-transform operation may be implemented in GPU (graphical processing unit) hardware to further reduce computation time.

6. CONCLUSION

We have described a novel FDTD updating formulation which enables the electric field of a Yee-grid simulation cell to respond according to X-Parameter data. These X-Parameter data may come from measurement information on a real-world microwave device. They may be derived from analytical expressions, or as in the case of the experiments described herein, they may be captured from a separate simulation. In all cases, the X-Parameters provide a common language by which the behavior of a nonlinear device may be captured, stored, and then applied to understand the behavior of a nonlinear device within the context of an overall system.

Presently, there are two primary mechanisms for embedding the functionality of a nonlinear device into the FDTD simulation. One approach is to write a specific FDTD updating equation based on the empirical model for the device, for example, a transistor. This approach has two drawbacks: first, it is challenging to fit empirical semiconductor models to measurement data unless measurements are conducted under a wide range of device operating conditions [5]. Second, it is not always possible to formulate an empirical semiconductor model in such a way that allows it to update an FDTD cell through a closed-form expression. In these cases, numeric approximations or iterative solution techniques are required. A second approach for embedding arbitrary circuits into FDTD simulations was described by Piket-May et al. [8], and uses a circuit interface between FDTD and a SPICE circuit simulator. However, this type of formulation does not take advantage of the central-difference, second-order approximation afforded by the FDTD technique. Simulations employing the suggested FDTD-SPICE approach must use extremely small time-steps relative to the simulated frequencies.

The X-Parameters provide a uniform means for characterizing a wide range of nonlinear devices: the same approach applies whether for a diode, junction transistor, or field-effect transistor, no matter the gate topology or material. We embedded the X-Parameter representation into the FDTD simulation in such a way as to take full advantage of the central-difference time-stepping approximation afforded by FDTD. Further, since the X-Parameters already linearize device behavior around a specified operating point, iterative solution of nonlinear equations is not required: only solution of a small linear system of equations.

Applications of this work include cases where it is desirable to simulate a nonlinear device within the context of a complex, 3D geometry. This approach provides a "one-shot" simulation, without the requirement to transfer data between multiple simulation engines (circuit simulator and EM) at each time step. Further work in this area will include the capability to automatically determine the amplitude and phase of the incoming A wave, and select the appropriate $LSOP$ condition and P phase, in cases where these values cannot be known in advance of the simulation.

REFERENCES

1. Elsherbeni, A. Z. and V. Demir, *The Finite-Difference Time-Domain Method For Electromagnetics with MATLAB Simulations*, The Institution of Engineering and Technology, Raleigh, 2016.
2. Kast, J. M. and A. Z. Elsherbeni, "Extraction of nonlinear X-Parameters from FDTD simulation of a one-port device," *2021 United States National Committee of URSI National Radio Science Meeting (USNC-URSI NRSM)*, 89–90, IEEE, 2021.

3. Kast, J. M. and A. Z. Elsherbeni, "Extraction of X-Parameters from FDTD simulation of a two-port nonlinear circuit," *2021 International Applied Computational Electromagnetics Society Symposium (ACES)*, 1–3, IEEE, 2021.
4. Kast, J. M. and A. Z. Elsherbeni, "FDTD simulation of nonlinear diode characteristics using X-Parameter-based updating formulation," *2021 1st International Conference on Microwave, Antennas & Circuits (ICMAC)*, 1–4, IEEE, 2021.
5. Kompa, G., *Parameter Extraction and Complex Nonlinear Transistor Models*, Artech House, Norwood, 2020.
6. Demir, V., "Formulations for modeling voltage sources with RLC impedances in the FDTD method," *Applied Computational Electromagnetics Society (ACES) Journal*, Vol. 31, No. 9, 1020–1027, 2016.
7. ElMahgoub, K. and A. Z. Elsherbeni, "FDTD implementations of integrated dependent sources in full-wave electromagnetic simulations," *Applied Computational Electromagnetics Society (ACES) Journal*, Vol. 29, No. 12, 1514–1523, 1994.
8. Piket-May, M., A. Taflove, and J. Baron, "FD-TD modeling of digital signal propagation in 3-D circuits with passive and active loads," *IEEE Transactions on Microwave Theory and Techniques*, Vol. 42, No. 8, 1514–1523, 1994.
9. Kung, F. and H. T. Chuah, "Modeling of bipolar junction transistor in FDTD simulation of printed circuit board," *Progress In Electromagnetics Research*, Vol. 36, 179–202, 2002.
10. Kuo, C., V. A. Thomas, S. T. Chew, B. Houshmand, and T. Itoh, "Small signal analysis of active circuits using FDTD algorithm," *IEEE Microwave and Guided Wave Letters*, Vol. 5, No. 7, 216–218, 1995.
11. Matteucci, M., P. Mezzanotte, L. Roselli, and P. Ciampolini, "Numerical analysis of electronic circuits with FDTD-LE technique," *WIT Transactions on Engineering Sciences*, Vol. 11, 197–204, 1996.
12. Kuo, C., B. Houshmand, and T. Itoh, "Full-wave analysis of packaged microwave circuits with active and nonlinear devices: An FDTD approach," *IEEE Transactions on Microwave Theory and Techniques*, Vol. 45, No. 5, 819–826, 1997.
13. Root, D. E., J. Verspecht, J. Horn, and M. Marcu, *X-Parameters: Characterization, Modeling, and Design of Nonlinear RF and Microwave Components*, Cambridge University Press, Cambridge, 2014.
14. Moon, T. K. and W. C. Stirling, *Mathematical Methods and Algorithms for Signal Processing*, Prentice Hall, Upper Saddle River, NJ, 2000.
15. Balanis, C., A., *Advanced Engineering Electromagnetics*, Wiley, Hoboken, NJ, 2012.
16. "ngSPICE," http://ngspice.sourceforge.net/.